RSC Applied Interfaces

Accepted Manuscript

This article can be cited before page numbers have been issued, to do this please use: C. Tian, C. Maheu, X. Huang, F. Oropeza, M. Major, J. Brötz, M. Einert, W. Donner, K. H. L. Zhang and J. P. Hofmann, *RSC Appl. Interfaces*, 2024, DOI: 10.1039/D4LF00260A.

ROYAL SOCIETY OF CHEMISTRY

rsc.li/RSCApplInter

View Article Online
DOI: 10.1039/D4LF00260A

ARTICLE

Evaluating the electronic structure and stability of epitaxially grown Sr-doped $LaFeO_3$ perovskite alkaline O_2 evolution model electrocatalysts

Received 00th January 20xx,
Accepted 00th January 20xx

DOI: 10.1039/x0xx00000x

Chuanmu Tian[a], Clément Maheu[a,b], Xiaochun Huang[c], Freddy E. Oropeza[d], Márton Major[e], Joachim Brötz[e], Marcus Einert[a], Wolfgang Donner[e], Kelvin Hongliang Zhang[c], Jan P. Hofmann[a]*

In this work, we have investigated the relationships between surface stability, electronic structure and O_2 evolution reaction (OER) activity for epitaxial thin film $La_{1-x}Sr_xFeO_3$ (x = 0, 0.33, 0.8) model electrocatalysts before and after different electrochemical treatments. Cyclic voltammetry (CV) between +1.22 V and +1.92 V vs. RHE results in the continuous enhancement of OER performance of $LaFeO_3$, while for $La_{0.67}Sr_{0.33}FeO_3$ and $La_{0.2}Sr_{0.8}FeO_3$ a gradual decrease of OER performance with increasing number of CV cycles was observed. A combination of atomic force microscopy, X-ray diffraction and X-ray reflectivity reveals that the surfaces of $La_{1-x}Sr_xFeO_3$ (x = 0, 0.33, 0.8) undergo surface morphology changes during OER treatment. Synchrotron ex-situ X-ray photoemission spectroscopy data show a gradual down-shift of the Fermi level (E_F) of $LaFeO_3$ with increasing number of CV cycles, while near edge X-ray absorption fine structure spectroscopy (NEXAFS) at the Fe L-edge and O K-edge shows the presence of surface Fe^{4+} species as well as new hole states near the conduction band minimum upon electrochemical treatment, leading to a further enhancement of the electrochemical activity of $LaFeO_3$. The newly formed hole state in $LaFeO_3$ that appeared after 3 CV cycles remained constant upon progressing OER treatment. On the contrary, the decrease of OER performance of $La_{0.67}Sr_{0.33}FeO_3$ and $La_{0.2}Sr_{0.8}FeO_3$ with increasing CV cycles is attributed to an up-shift of E_F along with a decrease of Fe^{4+} and hole state content after OER treatment. Furthermore, we found that the stability of the OER performance of $La_{1-x}Sr_xFeO_3$ is closely related to the leaching of Sr during OER, and the stability deteriorates with increasing Sr doping concentration in the pristine samples.

Introduction

Electrochemical water splitting is a promising pathway for large-scale production of green hydrogen and is expected to contribute to solving global energy and environmental issues.[1,2] However, the oxygen evolution reaction (OER) limits the efficiency of the overall water electrolysis due to the higher overpotential caused by the kinetically demanding four electron/proton transfer process.[3,4] Therefore, the development of highly active and stable OER electrocatalysts is critical to water electrolysis. Currently, IrO_2- and RuO_2-based catalysts for water electrolysis have been considered as the best OER catalysts in acidic media owing to their excellent OER activity, but their scarcity and high cost hinder their large-scale application.[5-7] Hence, cheap, earth-abundant and stable transition metal oxides are becoming more attractive, especially Fe, Co and Ni, when alkaline water electrolysis is considered.[8-10] Among them, the perovskite oxides have attracted great attention due to their low cost and tunable electronic structure.[11-13] Perovskite oxides have the general formula ABO_3, where A is an alkaline earth metal cation (La, Ba, Sr, etc.) and B is a transition metal cation (Fe, Co, Ni, etc.).[14] Currently, in order to provide a design basis for optimally performing semiconducting perovskite oxide OER electrocatalysts, significant efforts are devoted to explore the relationship between the electronic structure and electrocatalytic activity of perovskite oxides with activity descriptor concepts such as the e_g orbital occupancy,[15] p-band centre of the oxygen atom,[16] metal-oxygen covalency.[17]

$LaFeO_3$, a typical perovskite oxide, has been widely studied due to its good stability in alkaline electrolytes and adjustable electronic structure.[18,19] Over the past decades, a series of strategies has been explored to enhance the electrochemical activity of $LaFeO_3$, including nanostructure engineering to increase the surface area,[20] morphology design to expose more active crystal facets,[21] and aliovalent doping to increase the electrical conductivity and to modulate electronic structure.[22-25] Among them, aliovalent doping is a powerful method to enhance the OER activity of $LaFeO_3$. Recently, we found that doping by Sr can significantly improve the OER performance of $LaFeO_3$.[26] We argue that filled electronic states near the Fermi level (E_F) improve the orbital overlap with key OER reaction intermediates, favouring their formation. At the same time, the hole states close to the E_F increase the electron affinity of the $LaFeO_3$, thereby facilitating charge transfer at the

[a] Surface Science Laboratory, Department of Materials- and Geosciences, Technical University of Darmstadt, Peter-Grünberg-Straße 4, 64287 Darmstadt, Germany.
[b] Université de Nantes, CNRS, Institut des Matériaux Jean Rouxel, IMN, F-44000 Nantes, France.
[c] State Key Laboratory of Physical Chemistry of Solid Surfaces, College of Chemistry and Chemical Engineering, Xiamen University, Siming South Street 422, Xiamen 361005, P. R. China.
[d] Photoactivated Processes Unit, IMDEA Energy Institute, Parque Tecnológico de Móstoles, Avda. Ramón de la Sagra 3, 28935 Móstoles, Madrid, Spain.
[e] Department of Materials- and Geosciences, Technical University of Darmstadt, Peter-Grünberg-Straße 2, 64287 Darmstadt, Germany.
Supplementary Information available: [details of any supplementary information available should be included here]. See DOI: 10.1039/x0xx00000x

solid-electrolyte interface. Importantly, it has been observed that perovskite electrocatalysts usually undergo surface morphology and compositional changes during OER.[27-34] It is then almost impossible to predict the OER performance of electrocatalysts from their pristine (bulk and surface) composition and structure since their active surface phase can strongly differ from the bulk composition and structure.[35] Thus, it is critical to investigate the electronic structure and surface properties of the catalytically active surface, ideally under in-situ conditions. For example, Wan et al. reported that $SrIrO_3$ undergoes surface reconstruction accompanied by the formation of amorphous layers during electrochemical treatment.[36] They attributed the improved OER performance of $SrIrO_3$ to the formation of more active amorphous Sr_yIrO_x layer. Another typical perovskite with surface reconstruction is $Ba_{0.5}Sr_{0.5}Co_{0.8}Fe_{0.2}O_{3-\delta}$ (BSCF).[37] Fabbri et al. used in-situ X-ray absorption spectroscopy (XAS) to reveal that the (Co/Fe)O(OH) layer, which formed by the surface reconstruction of BSCF, can be considered as the OER active surface phase.

Although we have established the relationship between the electronic structure of pristine Sr-doped $LaFeO_3$ powder-based electrocatalysts and their OER activity[26], the stability of the surface chemical composition, morphology, and electronic structure as the OER progresses still needs to be investigated and verified. Therefore, in order to establish a relationship between the surface properties, i.e., surface chemical composition, atomic and electronic structure including their stabilities, and the OER activity of the Sr-doped $LaFeO_3$, we have employed epitaxial $La_{1-x}Sr_xFeO_3$ (001) single crystalline films as models to exclude the effect of nanostructure. We prepared a series of well-defined $La_{1-x}Sr_xFeO_3$ (x = 0, 0.33, 0.8) single crystal films on Nb-doped $SrTiO_3$ (001) substrate via pulsed laser deposition (PLD). Our result show that the OER performance of $LaFeO_3$ increases with increasing CV cycles, while the OER activity of $La_{0.67}Sr_{0.33}FeO_3$ and $La_{0.2}Sr_{0.8}FeO_3$ is gradually decreasing. The surface properties of $La_{1-x}Sr_xFeO_3$ (x = 0, 0.33, 0.8) were investigated by atomic force microscopy (AFM), X-ray diffraction (XRD) and X-ray reflectivity (XRR) before and after OER treatments. The combination of synchrotron X-ray photoemission spectroscopy (SXPS) and near edge X-ray absorption fine structure spectroscopy (NEXAFS) revealed electronic structure changes of $La_{1-x}Sr_xFeO_3$ (x = 0, 0.33, 0.8) upon OER treatment in the amount of surface Fe^{4+} active species, hole state and occupied density of states (DOS) near the Femi level (E_F).

Experimental section

Materials synthesis

$La_{1-x}Sr_xFeO_3$ (x = 0, 0.33, 0.8) targets were synthesized by solid-phase reaction. Stoichiometric amounts of La_2O_3 (Alfa, > 99.999%), Fe_2O_3 (Alfa, > 99.999%) and SrO (Alfa, > 99.999%) were mixed in a mortar. After grinding for 2 hours, the powder was pressed into pellets through a hydraulic press at 10 tons for 2 minutes, and finally these pellets were calcined in a muffle furnace (Kejing, KSL-1700) at 1000 °C for 24 h with 5 °C/min heating rate, followed by natural cooling to room temperature. $La_{1-x}Sr_xFeO_3$ (x = 0, 0.33, 0.8, 1.0) single crystal thin films were grown on one-side polished (001)-oriented 0.1% Nb-doped $SrTiO_3$ substrates (HeFei Kejing) by PLD using the respective target. Laser ablation was performed at a repetition rate of 5 Hz and an energy density of 1.0 J/cm² with a 248 nm KrF excimer laser. To achieve ~40 nm film thickness, the laser was impinged on the target for 15 min with the substrate temperature 550 °C and oxygen partial pressure of 30 mTorr.

View Article Online
DOI: 10.1039/D4LF00260A

Materials characterization

The crystal structure of the pure $La_{1-x}Sr_xFeO_3$ targets was analysed by X-ray diffraction (XRD) using Cu Kα radiation generated at 40 kV and 44 mA. Thin film growth was examined by high-resolution X-ray diffraction using a rotating Cu anode (45 kV, 190 mA) Rigaku SmartLab diffractometer in θ-2θ geometry, equipped with a Ge (220) double bounce monochromator (selecting the Cu $K\alpha_1$ wavelength) in parallel beam mode, while the thickness of the films was determined by X-ray reflectivity (XRR) scans on the same diffractometer. The surface morphology of the $La_{1-x}Sr_xFeO_3$ samples before and after OER treatments were determined by atomic force microscopy (AFM) with a Bruker Icon Dimension AFM in amplitude modulation mode using PPP-Zeihr cantilevers (NanoAndMore GmbH, Wetzlar, Germany). This type of cantilever has a nominal spring constant of 27 N/m, a nominal resonance frequency of 130 kHz, and a typical tip radius of <7 nm. A free oscillation amplitude $A_0 \approx$ 120 nm of the cantilever tip was adjusted, and a setpoint ratio of $A_{sp}/A_0 \approx 0.7$ was set to ensure operation in the repulsive tip–sample interaction regime. We scanned the surface with a tip velocity of 2 µm/s.

The SXPS and NEXAFS measurements were performed at the soft X-ray spectroscopy undulator beamline U49-2_PGM-1 at BESSY II synchrotron in Berlin. The beamline provides photons in the energy range of 85 – 1600 eV. The Solid-Liquid-Interface Analysis System (SOLIAS) endstation has been used and spectra were measured at normal emission using a Phoibos 150 (SPECS) energy analyser with a 1D delay line detector.[38] An Ar-ion sputter-cleaned Au foil served as a calibration sample by making use of the $Au4f_{7/2}$ transition located at 84.0 eV. Samples were electrically connected to the ground of the spectrometer. Excitation energies were adjusted for each core level to measure the photoelectrons at identical kinetic energy of 550 eV, which allows investigation of each element at a comparable depth of analysis, i.e., three times the inelastic mean free path at 550 eV kinetic energy (1.2-1.3 nm). The NEXAFS measurements at the Fe L-edge and O K-edge were carried out by recording the Auger electron yield of the respective elements.

Electrochemical measurements were carried out in three-electrode configuration using a Palmsens electrochemical workstation (Palmsens BV, The Netherlands) setup in the double glass cross electrochemistry chamber of the SOLIAS endstation.[38] The chamber was continuously purged by argon keeping the sample under an inert, dry, and carbon-free atmosphere and minimizing atmospheric contamination between the electrochemical treatments and the synchrotron-based measurements. A platinum wire was used as a counter electrode and Hg/HgO (1 M KOH) as a reference electrode. Cyclic voltammetry (CV) measurements were performed in 1 M KOH at a scan rate of 10 mV/s with the potential from +1.22 to +1.92 V (vs. RHE). Each sample was subjected to four OER treatments, namely total 0 CV (exposure to electrolyte only), total 3 CV (+3 increment), total 10 CV (+7 increment), and total 30 CV (+20 increment) cycles. After each treatment step, the sample was rinsed with MilliQ water and blown dry by Ar, then transferred to the vacuum system of the SOLIAS endstation for spectroscopic investigation.

Results and Discussion

Structural characterization

XRD and XRR were employed to characterize the quality of the $La_{1-x}Sr_xFeO_3$ thin films grown on 0.1% Nb-doped $SrTiO_3$ (001) substrates by PLD. Figure 1 shows the XRD and XRR results of the $La_{1-x}Sr_xFeO_3$ in pristine state (black curve) and after 30 CV cycles (i.e., after all four electrochemical treatment steps, red

View Article Online
DOI: 10.1039/D4LF00260A

curve). The well-defined oscillations are observed in both XRD and XRR plots for pristine $LaFeO_3$ (LFO) and $La_{0.67}Sr_{0.33}FeO_3$ (LSF-0.33), indicating the high quality of the thin films. However, these oscillations did not appear in the XRD plot (Figure 1c) of $La_{0.2}Sr_{0.8}FeO_3$ (LSF-0.8), which is attributed to the presence of a large number of oxygen vacancies in the LSF-0.8 sample causing the film not to grow epitaxial, similar as reported for $SrCoO_{3-x}$ and $SrFeO_{3-x}$.[39,40] The

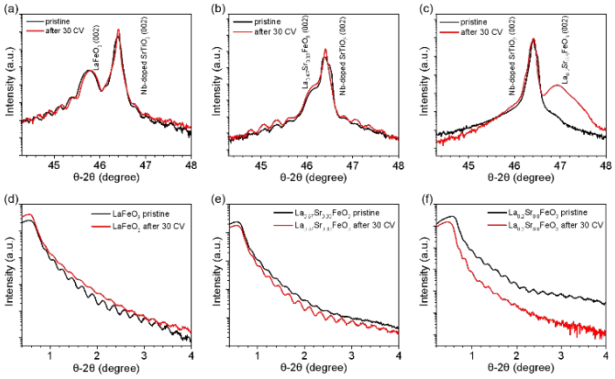

Figure 1. XRD and XRR of $La_{1-x}Sr_xFeO_3$ thin films in pristine state (black curves) and after 30 CV cycles (red curves). (a) XRD of $LaFeO_3$, (b) XRD of $La_{0.67}Sr_{0.33}FeO_3$, (c) XRD of $La_{0.2}Sr_{0.8}FeO_3$, (d) XRR of $LaFeO_3$, (e) XRR of $La_{0.67}Sr_{0.33}FeO_3$ and (f) XRR of $La_{0.2}Sr_{0.8}FeO_3$.

peak at 2θ = 46.4° corresponds to the (002) orientation of the 0.1% Nb-doped $SrTiO_3$ single crystal substrate, while the peaks at 2θ = 45.8°, 46.2° and 46.9° correspond to (002) oriented LFO, LSF-0.33 and LSF-0.8, respectively. To determine the thickness of the $La_{1-x}Sr_xFeO_3$ thin films, we obtained and fitted XRR data as shown in Figure S1, and the corresponding fitting parameters are reported in Table S1. The overall thickness of the pristine LFO, LSF-0.33 and LSF-0.8 single crystal thin films are 37.5 ± 0.5 nm, 38.6 ± 0.2 and 39.2 ± 0.2, respectively. After 30 CV cycles between +1.22 V to +1.92 V (vs. RHE) in 1 M KOH, there is a slight decrease in the thickness of the crystalline layer of all $La_{1-x}Sr_xFeO_3$ (x = 0, 0.33) thin films and an amorphous layer appears on all $La_{1-x}Sr_xFeO_3$ (x = 0, 0.33) film surfaces. The corresponding XRR plot of LFO before and after OER treatment is shown in Figure 1d. We also notice that the distance of the Kiessig fringes in the XRR plot of LFO remain consistent after 30 CV cycles, indicating negligible change of the overall film thickness. At the same time, the XRD (Figure 1b) and XRR (Figure 1e) data of LSF-0.33 show that the thickness of the crystalline layer as well as the overall thickness of the film remain unchanged. Figure 1c shows the XRD results of LSF-0.8 before and after 30 CV cycles; we notice that the peak intensity corresponding to LSF-0.8 increased after 30 CV, which is attributed to a surface reconstruction of LSF-0.8 thin film occurring under OER conditions. Based on the XRD and XRR results, we can state that the OER treatment resulted in an amorphous layer on the surface of $La_{1-x}Sr_xFeO_3$ (x = 0, 0.33) samples. In addition, Table S1 compiles the roughness of all $La_{1-x}Sr_xFeO_3$ (x = 0, 0.33, 0.8) samples. After 30 CV cycles, the roughness of LFO and LSF-0.33 increased from 0.61 nm to 0.69 nm and 0.67 to 0.82, respectively, while the roughness decreased from 1.73 nm to 0.41 nm for LSF-0.8.

To further investigate the effect of OER treatment on the surface properties, we carried out AFM measurements on the pristine and OER-treated thin films. As shown in Figures S2a and S2c, the pristine LFO and LSF-0.33 have a flat surface with a root mean square roughness (RMS) of 0.50 nm and 0.30 nm, respectively, which further confirms the high quality of these films grown by PLD. However, the RMS of pristine LSF-0.8 reaches 5.36 nm which is much higher than LFO and LSF-0.33. Such a high RMS value of LSF-0.8 is attributable to the fact that it was not epitaxially grown on the 0.1% Nb-$SrTiO_3$ substrate, which is consistent with the above XRD results. After all four OER treatment steps, the RMS of LFO (Figure S2b) remained virtually unchanged. As shown in Figure S2c, the RMS of LSF-0.33 increased from the initial 0.30 nm to 1.12 nm after OER treatment. On the contrary, we notice that the RSM of LSF-0.8 (Figure S2f) is drastically reduced from 5.36 to 0.54 nm after OER treatment. Among them, the changes in the LSF-0.8 film due to OER treatment were the most pronounced, which is consistent with our XRD and XRR results.

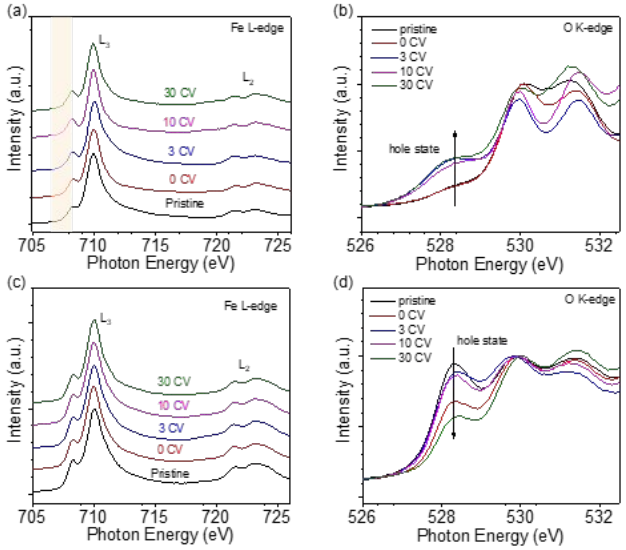

Figure 2. NEXAFS spectra of $LaFeO_3$ and $La_{0.67}Sr_{0.33}FeO_3$ with different CV cycles. (a) Fe L-edge of $LaFeO_3$, (b) O K-edge of $LaFeO_3$, (c) Fe L-edge of $La_{0.67}Sr_{0.33}FeO_3$ and (d) O K-edge of $La_{0.67}Sr_{0.33}FeO_3$. The yellow bars in Figure 2a indicate the changes in the characteristics of Fe^{3+} and Fe^{4+} at 708 eV under different CV cycles.

Electronic structure by X-ray photoemission and absorption spectroscopies

The oxidation state of Fe was determined by NEXAFS of the Fe L-edge. Figure 2a shows the Fe L-edge of LFO after different OER treatment steps. The shape of the spectra of pristine and 0 CV samples are consistent with previously reported results for Fe^{3+} oxidation state.[26] More importantly, the shape and intensity of the Fe L-edge remain consistent after 3 and even 30 CV cycles. To further investigate the oxidation state of Fe, we measured the O K-edge NEXAFS of LFO after different CV cycles, shown in Figure 2b. The results indicate that a new unoccupied (hole) state emerges at 528.4 eV, which is associated with Fe^{4+} in agreement with our previous report.[26] More interestingly, this hole state exhibits the same behaviour after 3 and even 30 CV cycles. The Fe L-edge of pristine samples of LSF-0.33 (Figure 2c, black curve) and LSF-0.8 (Figure S3a, black curve) also exhibited Fe^{4+} oxidation state characteristics, with LSF-0.8 being very similar to $SrFeO_3$. However, the linear shape and intensity of the Fe L-edge of LSF-0.33 and LSF-0.8 both show slight changes at different CV cycles, suggesting that the Fe^{4+} oxidation state still exists after OER treatment. At the same time, the intensity of the hole state features in the O K-edge spectra in LSF-0.33 (Figure 2d) and LSF-0.8 (Figure S3b) samples exhibit a gradually decreasing trend with increasing CV cycles,

View Article Online
DOI: 10.1039/D4LF00360A

indicating that the Fe^{4+} content in LSF-0.33 and LSF-0.8 is gradually decreasing due to the fact that these hole states are closely related to the Fe^{4+} oxidation state. Additionally, we still observe the presence of the hole state on the O K-edge even after 30 CV cycles, further confirming that Fe^{4+} is still existent in LSF-0.33 and LSF-0.8 after different OER treatment steps. Taken together, the above results indicate that the OER treatment led to a morphology change of the $La_{1-x}Sr_xFeO_3$ surface and the appearance of a hole state at LFO, while the hole state content of both LSF-0.33 and LSF-0.8 samples decreased after surface reconstruction.

In order to investigate the stability of the surface chemical composition and electronic structure of $La_{1-x}Sr_xFeO_3$ (x = 0, 0.33, 0.8) with increasing OER

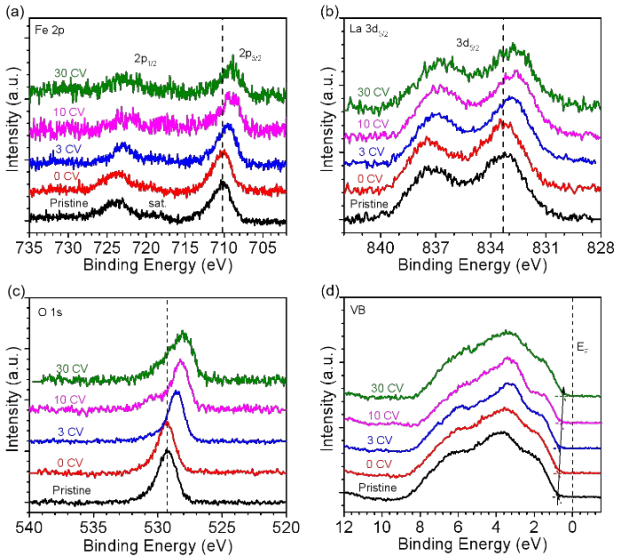

Figure 3. SXPS of $LaFeO_3$ with kinetic energy constant at 550 eV. (a) Fe 2p, (b) La 3d, (c) O 1s and (d) VB spectra after different CV cycles.

treatment steps, we additionally carried out synchrotron XPS (SXPS) measurements. Figure 3 shows the SXPS core level and VB spectra of LFO after different CV cycles; the XAS and XPS data have been acquired subsequently before each next OER treatment step. The Fe $2p_{3/2}$ region of LFO pristine exhibits a characteristic feature located around 710.2 eV along with a satellite

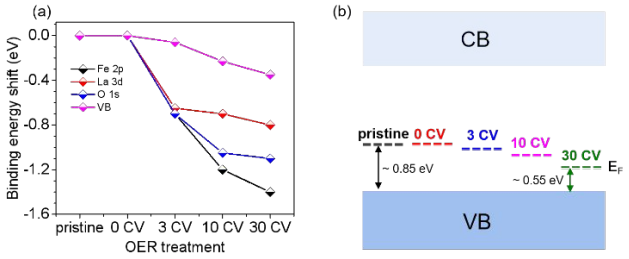

Figure 4. (a) Shifts of core level binding energy and (b) Fermi level (E_F) position of $LaFeO_3$ relative to the VBM BE as a function of CV cycles.

peak near 719 eV, in agreement with the Fe^{3+} oxidation state. After different OER treatments, the characteristics of Fe 2p did not change significantly, but the position of the main peak gradually shifted to lower binding energy with increasing CV cycles. The same shift is also seen in the corresponding La 3d (Figure 3b) and O 1s (Figure 3c) core level spectra. In addition, the VB spectrum of LFO in the Figure 3d show that the distance between the valence band maximum (VBM) and E_F decreased with increasing CV number, indicating a downward movement of E_F or alternatively an upward movement of the VBM.

Figure 4 summarizes the shift of the core levels and VB spectra, as well as the corresponding band energy schemes for LFO from the SXPS data. By combining the systematic shift of the binding energies of the Fe 2p, La 3d, and O 1s spectra together with the shift of the VB spectra, we can clarify the downward shift of E_F with progressing CV cycling. More importantly, the above XRD and AFM data combined with the NEXAFS results indicate that the shift of E_F can be attributed to the formation of Fe^{4+} species on the LFO surface due to surface reconstruction during the OER process. Such a phenomenon has also been observed in different transition metal oxides, such as, $LaNiO_3$ and $SrIrO_3$.[36,41] The SXPS data of LFO-0.33 with different numbers of CV cycles are shown in Figure S4, respectively. In contrast to the LFO samples, the core levels of LSF-0.33 (Fe 3d, La 3d, and O 1s) shift to higher binding energies, and the distance between VBM and E_F increased with increasing CV cycling, indicating a gradual upward movement of E_F in LSF-0.33.

Electrochemical characterization

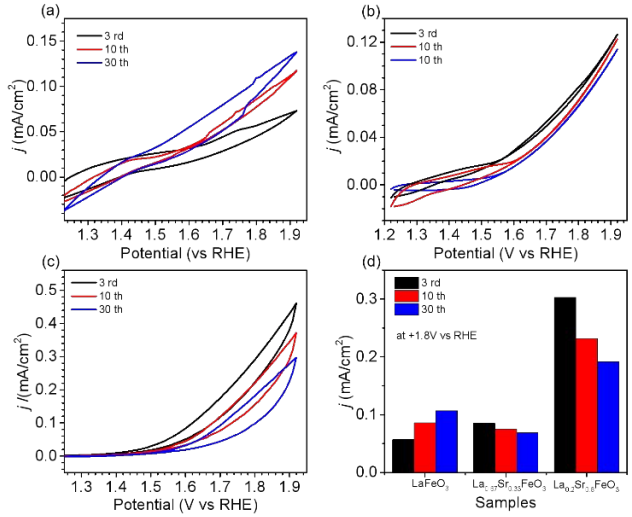

Figure 5. OER performance of $La_{1-x}Sr_xFeO_3$ with different CV cycles. (a) CV polarization curves of $LaFeO_3$, (b) CV polarization curves of $La_{0.67}Sr_{0.33}FeO_3$, (c) CV polarization curves of $La_{0.2}Sr_{0.8}FeO_3$ and (d) current density of $La_{1-x}Sr_xFeO_3$ (x = 0, 0.33, 0.8) with different CV cycles at +1.8 V (vs. RHE).

The OER performance of $La_{1-x}Sr_xFeO_3$ (x = 0, 0.33, 0.8) thin films were evaluated in a three-electrode setup in the double glass cross electrochemistry chamber of the SOLIAS endstation in 1 M KOH solution at 10 mV/s scan rate with a potential range of +1.22 V to +1.92 V vs RHE. The current density of CVs of all samples was normalized by the geometric area without ohmic compensation. Figure 5a shows CV plots of LFO under different CV cycles. The results suggest that the electrocatalytic activity of LFO experiences an enhancement with increasing number of CV cycles. On the contrary, the current density of LSF-0.33 (Figure 5b) as well as LSF-0.8 (Figure 5c) films show a continuous trend of decreasing OER performance. To compare the OER activity of $La_{1-x}Sr_xFeO_3$ with different Sr doping concentrations, the current densities of different samples with different CV cycles at +1.8 V (vs RHE) are shown in Figure 5d. The initial (3rd CV) OER

View Article Online
DOI: 10.1039/D4LF00260A

performance of $La_{1-x}Sr_xFeO_3$ is enhanced with increasing Sr doping concentration, which is in line with our previously reported results.[26] More importantly, we observed a more significant decrease in OER performance for the LSF-0.8 sample compared to LSF-0.33. The current density of LSF-0.33 at +1.8 V (vs RHE) decreases from 0.085 mA/cm² (3rd CV) to 0.069 mA/cm² (30th CV), while LSF-0.8 decreases from 0.303 mA/cm² (3rd CV) to 0.192 mA/cm² (30th CV) - a reduction of 18.8% and 41.8%, respectively.

It is well known that stability is also an important metric for evaluating OER catalysts. In order to have a more in-depth understanding of OER stability of the $La_{1-x}Sr_xFeO_3$ (x = 0, 0.33, 0.8) catalysts, we calculated the compositions of La, Sr and Fe (La%+Sr%+Fe%=100%) from SXPS spectral region integration after different CV cycles, as shown in Table 1. There is a significant increase in La concentration on the surface of the LFO film after OER treatment, which indicated that La gradually aggregated on the surface of LFO during the OER process. Recently, She et al. reported that surface aggregation of A-site cations (La or Sr) in $La_{1-x}Sr_xFeO_3$ is an important factor contributing to the poor OER

stability by blocking catalytically active sites.[22] In addition, we observe that the surface Sr content in both LSF-0.33 and LSF-0.8 gradually decreases with increasing CV, while the La content did not change significantly. The reduction of surface Sr concentration in LSF-0.33 and LSF-0.8 is related to the leaching of Sr during OER; a similar phenomenon has been observed in $SrIrO_3$.[36] There is a close relationship between current density and Sr concentration as shown in Figure 6. It can be clearly observed that the leaching of Sr in LSF-0.8 is particularly more pronounced as compared to LSF-0.33, in agreement with the deterioration of the OER performance.

Table 1. SXPS-derived (kinetic energy constant at 550 eV) La, Sr and Fe atomic compositions (La% + Sr% + Fe% = 100%) for $La_{1-x}Sr_xFeO_3$ (x = 0, 0.33, 0.8) with different CV cycles.

	LFO		LSF-0.33			LSF-0.8		
	La (at. %)	Fe (at. %)	La (at. %)	Sr (at. %)	Fe (at. %)	La (at. %)	Sr (at. %)	Fe (at. %)
Pristine[a]	50.0 ± 0.4	50.0 ± 0.2	33.5 ± 0.4	16.5 ± 0.6	50.0 ± 0.5	10.1 ± 0.2	40.0 ± 0.3	49.9 ± 0.3
0 CV[b]	49.1 ± 0.6	50.9 ± 0.3	33.9 ± 0.6	14.8 ± 0.3	51.2 ± 0.3	12.5 ± 0.3	36.4 ± 0.2	51.1 ± 0.4
3 CV[b]	62.6 ± 0.5	37.3 ± 0.4	33.0 ± 0.5	10.7 ± 0.4	55.7 ± 0.2	15.7 ± 0.5	22.7 ± 0.4	61.5 ± 0.2
10 CV[b]	63.0 ± 0.4	37.0 ± 0.5	31.5 ± 0.4	10.1 ± 0.5	58.4 ± 0.4	15.8 ± 0.4	17.2 ± 0.5	67.0 ± 0.4
30 CV[b]	64.5 ± 0.2	35.5 ± 0.4	31.1 ± 0.2	9.4 ± 0.4	59.5 ± 0.5	14.3 ± 0.2	15.1 ± 0.4	70.6 ± 0.5

[a] Expected stoichiometry

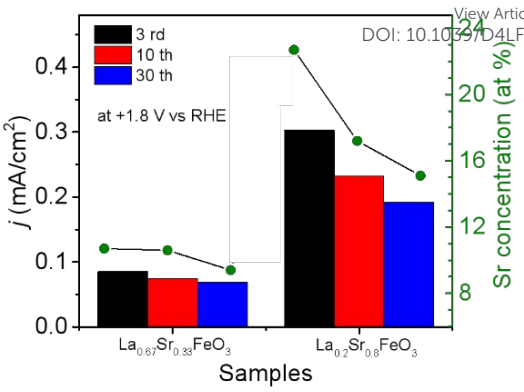

Figure 6. Relationship between current density and Sr concentration of $La_{0.67}Sr_{0.33}FeO_3$ and $La_{0.2}Sr_{0.8}FeO_3$ with different CV cycles.

[b] by XPS fitting

Such a different OER behaviour of $La_{1-x}Sr_xFeO_3$ with CV cycling is likely attributed to two factors. The first factor is the emergence of a hole state close to the conduction band minimum. Our recent study shows that the hole state near the conduction band minimum plays a crucial role in the oxidation of water by reducing the energy barrier for electron transfer at the electrode-electrolyte interface.[26] The above NEXAFS O K-edge spectra of LSF-0.33 and LSF-0.8 show that the content of the hole state (~528 eV) near the conduction band gradually decreases with increasing CV cycles, resulting in a decrease of OER performance. The second factor is the occupied density of states (DOS) near the E_F. According to the Marcus-Gerischer charge transfer model,[42] the increase in the occupied DOS near E_F would reduce the energy of donating electrons at the electrode-electrolyte interface, which results in increased performance of the catalyst by a decrease in charge transfer overpotential. It is worth noting that our SXPS results show that the E_F of LFO is shifting toward the VBM with increasing number of CV cycles, which indicates that the occupied DOS near the E_F is gradually increasing. On the contrary, the E_F of the LSF-0.33 shift away from the VBM, resulting in a decrease of occupied DOS near the E_F of LSF-0.33. The similar trend of electrochemical activity and occupied DOS near E_F indicates that occupied DOS near E_F are an important factor for determining the OER performance. Overall, our results highlight that the OER performance of $La_{1-x}Sr_xFeO_3$ (x = 0, 0.33, 0.8) is closely related to the surface Fe^{4+} species, the hole state near the CB and the occupied DOS near the E_F. Sr leaching during OER is the key factor for the poor stability of LSF-0.33 and LSF-0.8.

Conclusions

We have investigated the surface properties, stability of the electronic structure and OER performance of well-defined $La_{1-x}Sr_xFeO_3$ (x = 0, 0.33, 0.8) single crystal films. Our results reveal that operating the electrocatalysts under OER conditions lead to an increase of OER performance of LFO and a decrease of activity of LSF-0.33 and LSF-0.8. A combination of XRD, XRR and AFM measurements shows that the surfaces of $La_{1-x}Sr_xFeO_3$ (x = 0, 0.33, 0.8) undergo surface morphology and compositional changes upon OER treatment. Additionally, the electronic structure also experiences significant changes especially in the concentration of Fe^{4+} oxidation state, the hole state and the position of E_F with respect to the valence band maximum. The improved activity of LFO is attributed to i) the presence of hole states as well

as ii) the increase of the occupied density of states near E_F upon OER cycling. Conversely, the reduction of these factors leads to the decrease of OER performance of LSF-0.33 and LSF-0.8. The leaching of Sr is an important factor leading to the observed poor stability of LSF-0.33 and LSF-0.8 under OER conditions, and the OER performance decays faster with increasing Sr doping concentrations at the A-site in the pristine perovskite structure. Our study provides insights into the surface structural and compositional evolution, electronic structure stability and electrochemical properties of transition metal oxides as function of OER treatment and reveals that appropriate doping has substantial impact on the OER stability of transition metal oxides. The study further demonstrates the importance of synchrotron-based investigations for the precise determination and interpretation of electrochemical properties and activities with respect to electronic structure engineering of perovskite electrocatalysts achieving optimized OER performance.

Conflicts of interest

There are no conflicts to declare.

Data availability

Data supporting Figures and Tables in the manuscript and the Supporting Information is made available in a ZENODO.org repository accessible under DOI:XXX.XXX.XXX (%%will be provided upon acceptance of the manuscript%%).

Acknowledgements

Helmholtz Zentrum Berlin (HZB) is acknowledged for granting beam time at BESSY II under application 202-10001-ST-1.1-P. R. Golnak (HZB) is acknowledged for technical assistance during beam time at beamline U49-2_PGM-1. We also thank Dr. T. Hellmann and Dr. W. Calvet for setting up SOLIAS. C. M. Tian acknowledges financial support from the China Scholarship Council (No. 202008420222). J.P. Hofmann, M. Einert, and C. Maheu acknowledge financial support from the Deutsche Forschungsgemeinschaft (DFG, German Research Foundation under the Walter Benjamin Program to M. Einert, project no. 469377211 as well as in the priority program SPP2196, no. 423746744 and CRC 1548, FLAIR, project B07, no. 463184206).

References

1. Z. P. Ifkovits, J. M. Evans, M. C. Meier, K. M. Papadantonakis and N. S. Lewis, Decoupled Electrochemical Water-splitting Systems: A Review and Perspective, *Energy Environ. Sci.,* **2021**, 14, 4740.
2. L. Schlapbach and A. Züttel, Hydrogen-Storage Materials for Mobile Applications, *Nature,* **2001**, 414, 353-358.
3. Y. Gorlin and T. F. Jaramillo, A Bifunctional Nonprecious Metal Catalyst for Oxygen Reduction and Water Oxidation, *J. Am. Chem. Soc.,* **2010**, 132, 13612−13614.
4. E. Fabbri, A. Habereder, K. Waltar, R. Kotz and T. J. Schmidt, Developments and Perspectives of Oxide-Based Catalysts for the Oxygen Evolution Reaction, *Catal. Sci. Technol.,* **2014**, 4, 3800−3821.
5. V. Petrykin, K. Macounova, O. A. Shlyakhtin and P. Krtil, Tailoring the Selectivity for Electrocatalytic Oxygen Evolution on Ruthenium Oxides by Zinc Substitution, *Angew. Chem.Int. Ed.,* **2010**, 49, 4813−4815.
6. Y. Lee, J. Suntivich, K. J. May, E. E. Perry and Y. Shao-Horn, Synthesis and Activities of Rutile IrO_2 and RuO_2 Nanoparticles for Oxygen Evolution in Acid and Alkaline Solutions, *J. Phys. Chem. Lett.,* **2012**, 3, 399–404.
7. A. Zagalskaya and V. Alexandrov, Role of Defects in the Interplay between Adsorbate Evolving and Lattice Oxygen Mechanisms of the Oxygen Evolution Reaction in RuO_2 and IrO_2, *ACS Catal.,* **2020**, 10, 3650-3657.
8. N. T. Suen, S. F. Hung, Q. Quan, N. Zhang, Y. J. Xu and H. M. Chen, Electrocatalysis for the Oxygen Evolution Reaction: Recent Development and Future Perspectives, *Chem. Soc. Rev.,* **2017**, 46, 337.
9. W. T. Hong, M. Risch, K. A. Stoerzinger, A. Grimaud, J. Suntivich and Y. Shao-Horn, Toward the Rational Design of Non-Precious Transition Metal Oxides for Oxygen Electrocatalysis, *Energy Environ. Sci.,* **2015**, 8, 1404-1427.
10. K. X. Zhang and R. Q. Zou, Advanced Transition Metal-Based OER Electrocatalysts: Current Status, Opportunities, and Challenges, *Small,* **2021**, 17, 2100129.
11. D. Liu, P. F. Zhou, H. Y. Bai, H. Q. Ai, X. Y. Du, M. P. Chen, D. Liu, W. Fai, K. H. Lo, C. T. Kwok, S. Chen, S. P Wang, G. C. Xing, X. S. Wang an H. Pan, Development of Perovskite Oxide-Based Electrocatalysts for Oxygen Evolution Reaction, *Small,* **2021,** 17, 2101605.
12. C. W. Sun, J. A. Alonso and J. J. Bian, Recent Advances in Perovskite-Type Oxides for Energy Conversion and Storage Applications, *Adv. Energy Mater.,* **2021**, 11, 20000549.
13. H. N. Sun, J. Dai, W. Zhou and Z. P. Shao, Emerging Strategies for Developing High-Performance Perovskite-Based Materials for Electrochemical Water Splitting, *Energy Fuels,* **2020**, 34, 10547−10567.
14. X. Xu, C. Su, W. Zhou, Y. Zhu, Y. Chen and Z. Shao, Co-doping Strategy for Developing Perovskite Oxides as Highly Efficient Electrocatalysts for Oxygen Evolution Reaction, *Adv. Sci.,* **2016**, 3, 1500187.
15. J. Suntivich, K. J. May, H. A. Gasteiger, J. B. Goodenough and Y. Shao-Horn, A Perovskite Oxide Optimized for Oxygen Evolution Catalysis from Molecular Orbital Principles, *Science,* **2011**, 334, 1383−1385.
16. Y. L. Lee, J. Kleis, J. Rossmeisl, Y. Shao-Horn and D. Morgan, Prediction of Solid Oxide Fuel Cell Cathode Activity With First-Principles Descriptors, *Energy Environ. Sci.*, **2011**, 4, 3966-3970.
17. J. J. Song, C. Wei, Z. F. Huang, C. T. Liu, L. Zeng, X. Wang and Z. C. J. Xu, A Review on Fundamentals for Designing Oxygen Evolution Electrocatalysts, *Chem. Soc. Rev.*, **2020**, 49, 2196-2214.
18. A. R. Burton, R. Paudel, B. Matthews, M. Sassi, S. R. Spurgeon, B. H. Farnum and R. B. Comes, Thickness Dependent OER Electrocatalysis of Epitaxial $LaFeO_3$ Thin Films, *J. Mater. Chem. A*, **2022**, 10, 1909-1918.
19. Y. W. Dai, J. Yu, Z. B. Zhang, C. Cheng, P. Tan, Z. P. Shao and M. Ni, Interfacial La Diffusion in the CeO_2/$LaFeO_3$ Hybrid for Enhanced Oxygen Evolution Activity, *ACS Appl. Mater. Interfaces,* **2021**, 13, 2799–2806.
20. Y. X. Li, X.Y. Zhang, Z. J. Wu, H. B. Sheng, C. Li, H. Y. Li, L. X. Cao and B. H. Dong, Coupling Porous Ni Doped LaFeO3 Nanoparticles with Amorphous FeOOH Nanosheets Yields an Interfacial Electrocatalyst for Electrocatalytic Oxygen Evolution, *J. Mater. Chem. A*, **2021**, 9, 23545-23554.
21. J. Dai, Y. L. Zhu, Y. J. Zhong, J. Miao, B. W. Lin, W. Zhou and Z. P. Song,

Enabling High and Stable Electrocatalytic Activity of Iron-Based Perovskite Oxides for Water Splitting by Combined Bulk Doping and Morphology Designing, *Adv. Mater. Interfaces,* **2019**, 6, 1801317.

22. S. X. She, J. Yu, W. Q. Tang, Y. L. Zhu, Y. B. Chen, J. Sunarso, W. Zhou and Z. P. Shao, Systematic Study of Oxygen Evolution Activity and Stability on $La_{1-x}Sr_xFeO_{3-\delta}$ Perovskite Electrocatalysts in Alkaline Media, *ACS Appl. Mater. Interfaces*, **2018**, 10, 11715−11721.
23. Z. S. Li, L. Lv, J. S. Wang, X. Ao, Y J. Ruan, D. Z. Zha, G. Hong, Q. H. Wu, Y. C. Lan, C. D. Wang, J. J. Jiang and M. L. Liu, Engineering Phosphorus-doped $LaFeO_{3-\delta}$ Perovskite Oxide as Robust Bifunctional Oxygen Electrocatalysts in Alkaline Solutions, *Nano Energy,* **2018***,* 47, 199-209.
24. P. Shikha, T. S. Kang and B. S. Randhawa, Effect of Different Synthetic Routes on the Structural, Morphological and Magnetic Properties of Ce Doped $LaFeO_3$ Nanoparticles, *J. Alloys Compd.,* **2015**, 625, 336-345.
25. R. A. Rincón, E. Ventosa, F. Tietz, J. Masa, S. Seisel, V. Kuznetsov and W. Schuhmann, Evaluation of Perovskites as Electrocatalysts for theOxygen Evolution Reaction, *ChemPhysChem*, **2014**,15, 2810 – 2816.
26. Z. C. Shen, Y. B. Zhuang, W. W. Li, X. C Huang, F. E. Oropeza, E. J. M. Hensen, J. P. Hofmann, M. Y. Cui, A. Tadich, D. C. Qi, J. Cheng, J. Li and K. H. L. Zhang, Increased Activity in the Oxygen Evolution Reaction by Fe^{4+}-induced Hole States in Perovskite $La_{1-x}Sr_xFeO_3$, *J. Mater. Chem. A*, **2020**, 8, 4407–4415.
27. P. P. Lopes, D. Y. Chung, X. Rui, H, Zheng, H. Y. He, P. F. B. D. Martins, D. Strmcnik, V. R. Stamenkovic, P. Zapol, J. F. Mitchell, R. F. Klie and N. M. Markovic, Dynamically Stable Active Sites from Surface Evolution of Perovskite Materials during the Oxygen Evolution Reaction, *J. Am. Chem. Soc.*, **2021**, 143, 2741−2750.
28. J. J. Suo, B. W. Yang, E. Mosconi, H. S. Choi, Y. J. Kim, S. M. Zakeeruddin, F. D. Angelis, M. Grätzel, H. S. Kim and A. Hagfeldt, Surface Reconstruction Engineering with Synergistic Effect of Mixed-Salt Passivation Treatment Toward Efficient and Stable Perovskite Solar Cells, *Adv. Funct. Mater.,* **2021**, 31, 2102902.
29. Y. Sun, R. Li, X. X. Chen, J. Wu, Y. Xie, X. Wang, K. K. Ma, L. Wang, Z. Zhang, Q. L. Liao, Z. Kang and Y. Zhang, A-Site Management Prompts the Dynamic Reconstructed Active Phase of Perovskite Oxide OER Catalysts, *Adv. Energy Mater.,* **2021**, 11, 2003755.
30. L. K. Gao, X. Cui, C. D. Sewell, J. Li and Z. Q. Lin, Recent Advances in Activating Surface Reconstruction for the High-Efficiency Oxygen Evolution Reaction, *Chem. Soc. Rev.*, **2021**, 50, 8428.
31. A. Grimaud, A. Demortiere, M. Saubanere, W. Dachraoui, M. Duchamp, M. L. Doublet and J. M. Tarascon, Activation of Surface Oxygen Sites on an Iridium-Based Model Catalyst for the Oxygen Evolution Reaction, *Nat. Energy,* **2016***,* 2, 1-10.
32. Y. Sun, C. R. Wu, T. Y. Ding, J. Gu, J. W. Yang, J. Cheng and K. H. L. Zhang, Direct Observation of the Dynamic Reconstructed Active Phase of Perovskite LaNiO3 for the Oxygen-Evolution Reaction, *Chem. Sci.,* **2023,** 14, 5906-5911.
33. M. J. Choi, L. Wang, K. A, Stoerzinger, S. Y. Chung, S. A. Chambers and Y. G. Du, Epitaxial Design of Complex Nickelates as Electrocatalysts for the Oxygen Evolution Reaction, *Adv. Energy Mater.,* **2023,** 13, 2300239.
34. E. M. Kiens, M. J. Choi, L. H. Wei, Q. Y. Lu, L. Wang and C. Baeumer, Deeper Mechanistic Insights into Epitaxial Nickelate Electrocatalysts for the Oxygen Evolution Reaction, *Chem. Commun.,* **2023,** 59, 4562-4577. 35.
35. Y. Y. Li, X. C. Du, J. W. Huang, C. Y. Wu, Y. H. Sun, G. F. Zou, C. T. Yang and J. Xiong, Recent Progress on Surface Reconstruction of Earth-Abundant Electrocatalysts for Water Oxidation, *Small*, **2019**, 15, 1901980.
36. G. Wan, J. W. Freeland, J. Kloppenburg, G. Petretto, J. N. Nelson, D. Y. Kuo, C. J. Sun, J. G. Wen, J. T. Diulus, G. S. Herman, Y. Q Dong, R. H. Kou, J. Y. Sun, S. Chen, K. M. Shen, D. G. Schlom5, G. M. Rignanese, G. Hautier, D. D. Fong, Z. X. Feng, H. Zhou and J. Suntivich, **A**morphization Mechanism of $SrIrO_3$ Electrocatalyst: How Oxygen Redox Initiates Ionic Diffusion and Structural Reorganization, *Sci. Adv.,* **2021**, 7, 7323.
37. E. Fabbri, M. Nachtegaal, T. Binniger, X. Cheng, B. J. Kim, J. Durst, F. Bozza, T. Graule, R. Schäublin, L. Wiles, M. Pertoso, N. Danilovic, K. E. Ayers and T. J. Schmidt, Dynamic Surface Self-Reconstruction is the Key of Highly Active Perovskite Nano-Electrocatalysts for Water Splitting, *Nat. Mater.,* **2017***,* 16, 925-931.
38. T. Mayer, M. Lebedev, R. Hunger and W. Jaegermann, Elementary Processes at Semiconductor/Electrolyte Interfaces: Perspectives and Limits of Electron Spectroscopy, *Appl. Surf. Sci.,* **2005,** 252, 31-42.
39. S. J. Callori, S. Hu, J. Bertinshaw, Z. J. Yue, S. Danilkin, X. L. Wang, V. Nagarajan, F. Klose, J. Seidel and C. Ulrich, Strain-Induced Magnetic Phase Transition in $SrCoO_{3-\delta}$ Thin Films, *Phys. Rev. B,* **2015**, 91, 140405.
40. S. Roh, S. Lee, M. Lee, Y. S. Seo, A. Khare, T. Yoo, S. Woo, W. S. Choi and J. Hwang, Oxygen Vacancy Induced Structural Evolution of $SrFeO_{3-x}$ Epitaxial Thin Film from Brownmillerite to Perovskite, *Phys. Rev. B*, **2018**, 97, 075104.
41. H. Liu, R. R. Xie, Q. X. Wang, J. L. Han, Y. Han, J. Wang, H. Fang, J. Qi, M. Ding, W. X. Ji, B. He, W. M. Lü, Enhanced OER Performance and Dynamic Transition of Surface Reconstruction in $LaNiO_3$ Thin Films with Nanoparticles Decoration, *Adv. Sci.,* **2023**, 2207128.
42. I. Heller, J. Kong, K. A. Williams, C. Dekker and S. G. Lemay, Electrochemistry at Single-Walled Carbon Nanotubes: The Role of Band Structure and Quantum Capacitance, *J. Am. Chem. Soc.,* **2006**, 22, 7353–7359.

View Article Online
DOI: 10.1039/D4LF00260A

Data availability

Data supporting Figures and Tables in the manuscript and the Supporting Information is made available in a ZENODO.org repository accessible under DOI:XXX.XXX.XXX (%%will be provided upon acceptance of the manuscript%%).